Design for a High-resolution Small-Animal SPECT System Using Pixellated Si(Li) Detectors for *In Vivo* ^{125}I Imaging

W.-S. Choong, *Member, IEEE*, W. W. Moses, *Senior Member, IEEE*, C. S. Tindall, and P. N. Luke

***Abstract*— We propose a design for a high-resolution single-photon emission computed tomography (SPECT) system for *in vivo* ^{125}I imaging in small animal using pixellated lithium-drifted silicon (Si(Li)) detectors. The proposed detectors are expected to have high interaction probability (>90%), good energy resolution (<15% FWHM), and good intrinsic spatial resolution (~1 mm FWHM). The SPECT system will consist of a dual head detector geometry with the distance between the detectors ranging 30-50 mm to minimize the imaging distance between the mouse and the detectors. The detectors, each with an active area of 64 mm × 40 mm (64 × 40 array of 1 mm^2 pixels and a 6 mm thick Si(Li) detector), will be mounted on a rotating gantry with an axial field-of-view of 64 mm. The detector signals will be read out by custom application-specific integrated circuits (ASICs). Using a high-resolution parallel-hole collimator, the expected spatial resolution is 1.6 mm FWHM at an imaging distance of 20 mm, and sensitivity is 6.7 cps/μCi. ^{125}I is a readily available radioisotope with a long half-life of 59.4 days and it is commonly used to label biological compounds in molecular biology. Conventional gamma cameras are not optimized to detect the low emission energies (27 to 35 keV) of ^{125}I. However, Si(Li) detector provides an ideal solution for detecting the low-energy emissions of ^{125}I. In addition to presenting the design of the system, this paper presents a feasibility study of using Si(Li) detectors to detect the emissions of ^{125}I.**

***Index Terms*— small-animal, SPECT, lithium-drifted silicon (Si(Li)), pixellated detector, iodine-125, *in vivo*.**

I. Introduction

In recent years, small animal imaging has been the subject of intense research and development. This is largely due to the advances in molecular and cell biology, the use of transgenic mice models and the availability of new imaging tracers. The genetic similarity of mice to humans has enabled a wide range of human diseases to be studied in animal models. The completion of the sequence of the human genome [1] and mouse genome [2] will improve our understanding of human biology at the molecular level, and may enable us to create new and improved models of human diseases. Transgenic mice have been widely used in the study of cancer mechanisms and for modeling human diseases. Recently, the study of transgenic mice has opened new prospects in evaluating human gene therapy by noninvasive, repetitive and quantitative imaging of gene expression. Study methods for small animals include [3]: (1) imaging gene expression and regulation to reflect specific cellular and molecular processes; (2) imaging cell trafficking to understand the molecular pathways of many diseases; and (3) imaging during gene therapy to assess the effectiveness of the gene transduction.

The purpose of this paper is to provide a conceptual design for a single-photon emission computed tomography (SPECT) camera optimized for ^{125}I imaging of mice, and to evaluate the feasibility of using Si(Li) as the detector material.

II. ^{125}I Imaging in Small Animals

One of the most common single-photon radioisotopes used in human nuclear imaging is ^{99m}Tc, which emits a single 140 keV photon. As a result, conventional gamma cameras are optimized to detect the emissions from ^{99m}Tc. However, for small-animal imaging, it is possible to use a radioisotope that emits lower energy photons. ^{125}I decays via electron capture with the emission of a 35 keV gamma ray. Several K shell X-rays with photon energies ranging from 27 to 32 keV from the ^{125}Te daughter product can accompany the decay. The three highest photon emission probabilities for ^{125}I decay are 76% at 27.5 keV, 13% at 31 keV, and 7% at 35 keV [4]. These gamma rays have an average path-length of about 2 cm in soft tissue, which provides a sufficient transmission probability for the photon to escape from the body of the small animal. In addition, ^{125}I has a half-life of 59.4 days, and is already widely used in molecular biology research.

There are a number of advantages of using ^{125}I for small-animal imaging. First, many ^{125}I-labeled nucleic acids, antibodies, ligands, and other radiopharmaceuticals are commercially available [5, 6]. In addition, many other ^{125}I-labeled imaging probes can be readily synthesized using commercial iodination reagents and kits. Second, ^{125}I-labeled biological compounds or imaging probes can be readily replaced with another iodine radioisotope without changing their chemical and biological properties. One possible replacement is ^{123}I, which emits a higher photon energy (159 keV) that is more appropriate for SPECT imaging in humans. Another possible replacement is ^{124}I, which is a

Manuscript received Nov 15, 2003; revised Jun 8, 2004. This work was supported in part by the U.S. Department of Energy under contract No. DE-AC03-76SF00098.

The authors are with the Lawrence Berkeley National Laboratory, Berkeley, CA 94720 USA (telephone: 510-486-6757, e-mail: wschoong@lbl.gov).

positron emitter that can be used in positron emission tomography (PET) imaging. The ability to directly translate the research and techniques developed from small-animal imaging to clinical use is an important advantage. Finally, the long half-life makes radiolabeling work more convenient and also permits the study of gene expression products to be performed over an extended period of time in the same animal. However, in some cases, such long half-life can pose a problem because the iodine stays in the animal and continues to emit a strong signal, making repeat studies difficult. In instances where a short half-life of the radioisotope is needed, one possible solution is to replace ^{125}I with ^{123}I, which has a half-life of 13.2 hours. ^{123}I has a gamma-ray emission at 159 keV, but also results in the emission of the K shell X-rays of the ^{125}Te daughter product in the 27–32 keV range. For these reasons, *in vivo* ^{125}I imaging in small animals is very attractive and has motivated several groups to develop dedicated systems toward this goal [7-13].

III. Si(Li) Detectors

Although silicon (Si) is not normally considered for use as a gamma-ray detector because of its low density and atomic number, its properties are quite favorable for ^{125}I imaging. Because of the low-energy emissions of ^{125}I, Si has similar absorption length for 27 keV photons (~2.36 mm) as thallium-doped cesium iodide (CsI(Tl)) has for 140 keV photons. In addition, Si also has an adequate photoelectric fraction (80%) for the emissions of ^{125}I. While detectors fabricated from high-resistivity Si are commercially available, their thickness is limited to a maximum of about 2 mm. In order to get good interaction probability (~90%), the thickness of the silicon has to be greater than 5 mm. Thicker detectors can be achieved by using lithium-drifted silicon (Si(Li)) detectors. The process of drifting lithium into the silicon compensates for the impurities in silicon, thereby creating a bulk of "intrinsic" silicon, which can be made up to 1 cm thick. Si(Li) detectors have been made for over 40 years. The physics is very well understood and the basic fabrication process is a very mature technology. Other advantages of using Si(Li) include the ability to fabricate large active area detectors (10 cm × 10 cm) and the availability of many resources for processing silicon. Improved techniques for fabricating multi-electrode Si(Li) detectors have recently been developed [14]. We believe Si(Li) detectors offer the ideal solution for *in vivo* ^{125}I imaging.

Scintillator-based detectors have been used in nuclear imaging since the beginning of the field. Most of the development in conventional gamma camera is optimized for photon energies between 140 keV to 511 keV. The developments in position-sensitive photomultiplier tubes (PSPMTs) and scintillator arrays such as thallium-doped sodium iodide (NaI(Tl)) and CsI(Tl) have allowed the development of high-resolution compact gamma detectors. However, because of the low-energy emissions of ^{125}I, it has been reported that the energy resolution from exciting NaI(Tl) crystals coupled to PSPMTs with the emissions of ^{125}I was about 32% FWHM for a pixellated crystal and 26% FWHM for a single continuous crystal [15]. On the other hand, the direct conversion of the photon energy in a Si(Li) detector yields a large signal, and therefore the energy resolution of a Si(Li) detector is expected to be better than that of a scintillator-based detector for the emissions of ^{125}I. Other semiconductor detectors such as germanium (Ge) and cadmium zinc telluride (CdZnTe) detectors also give good energy resolution. However, Si(Li) detectors offer distinct advantages over these other semiconductor detectors. Operation of Ge detectors requires cryogenic temperature (~77K). Si has higher bandgap than Ge, allowing Si(Li) detectors to be operated at room temperature, which is impossible for Ge detectors because of the large thermally-induced leakage current. CdZnTe is a high Z, wide bandgap semiconductor that allows operation at room temperature with low leakage current. However, the reliable production of a large area CdZnTe detectors (> several cm^2) is fairly difficult due to crystal inhomogeneity and the low yield of single-crystal material. A large active area detector can be constructed by tiling detectors together, but dead area is introduced between the detectors. Another advantage of using Si over CdZnTe is that the energy required to create an electron-hole pair is lower in Si than in CdZnTe, so the signal contribution to the energy resolution in better in Si. Table I compares the properties of Si, Ge, and CdZnTe [16–18].

TABLE I
PROPERTIES OF SEMICONDUCTOR MATERIALS AT ROOM TEMPERATURE

Material	Si	Ge	CdZnTe
Atomic number	14	32	48/30/52
Energy gap (eV)	1.115	0.746 [b]	1.64
Energy/e-h pair (eV)	3.6	2.96 [b]	5.0
Photoelectric Fraction @ 27 keV	0.84	0.97	0.97
Photoelectric Fraction @ 35 keV	0.74	0.95	0.97
Absorption Length @ 27 keV (mm)	2.36	0.11	0.07
Absorption Length @ 35 keV (mm)	4.45	0.21	0.07
Electron Mobility (cm^2/V.s)	1350	3900	1000-1100 [a]
Hole Mobility (cm^2/V.s)	480	1900	50 [a]
Electron Lifetime (s)	2.5×10^{-3}	$\geq 10^{-4}$ [b]	$0.8\text{-}8 \times 10^{-6}$ [a]
Hole Lifetime (s)	2.5×10^{-3}	$\geq 10^{-4}$ [b]	$60\text{-}600 \times 10^{-9}$ [a]

All numbers are from [16] and [17], except otherwise stated.
[a] Taken from [18].
[b] At 77 K.

IV. System Design

We propose a design for a high-resolution SPECT system for *in vivo* ^{125}I imaging in small animals using Si(Li) detectors as the gamma-ray imaging detectors. As shown schematically in Fig. 1, the SPECT system consists of a dual head detector geometry that will be mounted on a rotating gantry. Each detector head will consist of a single, pixellated, monolithic Si(Li) detector with an active area of 64 mm x 40 mm. The detector is expected to have high interaction

probability (>90%), good energy resolution (<15% FWHM), and good intrinsic spatial resolution (~1 mm FWHM) for the emissions of ^{125}I.

The design of the detector head is shown in Fig. 2. Each detector head will consist of the pixellated Si(Li) detector that will be mounted on the detector module board, providing the electrical connections between the detector and the front-end readout boards. Each front-end readout board will have two application-specific integrated circuits (ASICs) to read out the detector signals. Each front-end readout board will plug into a detector head motherboard that provides the control signals, processes the output signals, and sends the data to the computer.

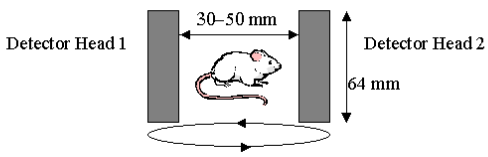

Fig. 1. Proposed dual head SPECT system rotating around the mouse.

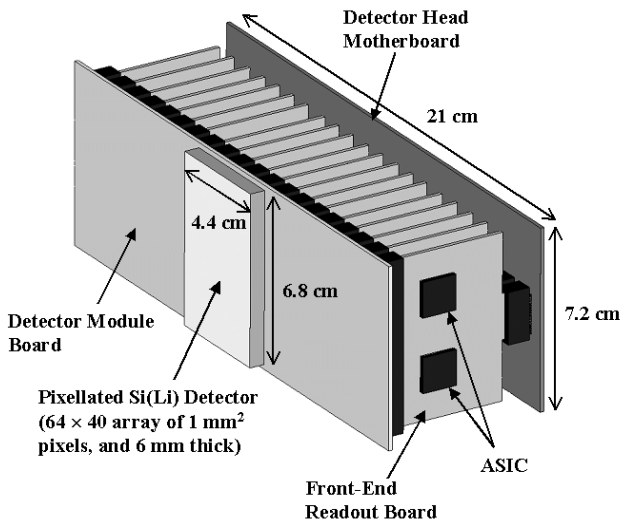

Fig. 2. Design of the proposed detector head.

A. Pixellated Si(Li) Detectors

Each of the proposed pixellated Si(Li) detector will be an array of 64 × 40 pixels, each 1 mm^2. In practice, there will be a gap between the pixel electrodes of about 50–100 μm. When a gamma ray interacts within the gap, the generated electron-hole pairs will be swept towards the closest electrode by the electric field created by the bias voltage. Thus, there is effectively no dead volume and very little cross talk between the pixels even though pixel area is smaller than 1 mm^2. Therefore, we expect the intrinsic spatial resolution to be equal to the pitch between the pixels, which is 1 mm. The thickness of the detector will be 6 mm, which is sufficient (for silicon) to achieve greater than 90% interaction probability for the emissions of ^{125}I. The detector will be fabricated at Lawrence Berkeley National Laboratory (LBNL) using the standard LBNL Si(Li) process, which has been described in [19, 20]. A new robust contact recently developed at LBNL [14] will be used to segment one side of the detector into a 64 x 40 array of 1 mm^2 pixels. A guard ring structure around the array of pixels will be fabricated to sink surface leakage current.

While Si(Li) detectors are usually cooled in order to reduce the leakage current, the pixel size in this design is small enough to allow room temperature operation. The bulk leakage current of each pixel is given by [21]

$$I = \frac{q n_i W}{2\tau_o} \tag{1}$$

where q is the equivalent charge (1.6×10^{-19} C), n_i is the intrinsic carrier concentration (1.5×10^{10} cm^{-3} at room temperature), W is the depleted volume (1 mm × 1 mm × 6 mm), and τ_o is the carrier lifetime (about 2.5 ms). The expected bulk leakage current in each pixel is therefore about 3 nA at room temperature. The compensated region of the Si(Li) detector is stable and can be operated at room temperature. Should the room-temperature leakage current be higher than expected, or should lower leakage current be desired, the detector could be cooled to reduce the leakage current. The amount of cooling required is likely to be no more than 50 °C below room temperature [14], which is possible using thermoelectric coolers.

B. Readout Electronics

The readout of a large number of high-density pixels will be accomplished by the use of readout ASICs. The readout ASIC will be based on a previous design [22], which is a mixed analog-digital design fabricated in CMOS (HP 0.5 μm 3.3 V technology) and covering an area of 4.5 mm x 4.8 mm. Its front-end is an array of 64 analog input channels consisting of charge-sensitive preamplifiers and shaper amplifiers. It is then followed by a "Winner Take All" (WTA) circuitry that reduces the 64 amplified, shaped signals to a single analog signal with the largest amplitude plus 6 digital bits that identify the winning channel.

The charge-sensitive preamplifier of the readout ASIC is optimized for an input load of about 5 pF. The re-designed ASIC must be optimized for the input capacitive load of our proposed detector. Since the detector capacitance is small (<1 pF) due to the small pixel size and large thickness, the dominant capacitance comes from routing some of the detector signals from the detector to the edge of the detector module board where the ASICs reside (~10 cm). Taking a conservative approach, we assume that the traces on the detector module board act like a strip detector with a strip pitch of about 100 μm (a reasonable spacing between copper traces in the fabrication of printed circuit board), yielding a strip-to-strip fringing capacitance of about 0.5 pF/cm. A typical strip will have fringing capacitances on both sides of the strip, resulting in a strip capacitance of about 1 pF/cm. Allowing for an additional 2 pF of parasitic capacitance from other sources (e.g. connection between the front-end readout board and the detector module board), we estimate that the total maximum capacitance shunting the input of the charge-sensitive preamplifier will be about 12 pF.

C. System Spatial Resolution and Sensitivity

Mechanical collimation is employed in gamma camera imaging using parallel-hole or pinhole collimators. However, the collimator is the limiting factor for both the spatial resolution and sensitivity. Different applications require different spatial resolution and sensitivity tradeoffs, which can be obtained easily by changing collimators. As these tradeoffs are well understood, we don't explore them in detail here. Instead, we use representative collimator parameters and estimate the system spatial resolution and sensitivity with our proposed detectors. Using the formulation developed in [23, 24] for pinhole collimators and [25, 26] for parallel-hole collimators, we calculated the system spatial resolution and sensitivity of tungsten pinhole and parallel-hole collimators for 27.5 keV photons as a function of the diameter of the pinhole and width of the square hole respectively for different imaging distances appropriate for mice imaging. The results are shown in Fig. 3 and Fig. 4 for pinhole and parallel-hole collimators respectively.

Recently, there has been an enormous interest in pinhole SPECT system for small animal imaging. Pinhole collimators can yield good system spatial resolution for SPECT because the spatial resolution is dominated by the pinhole diameter (essentially independent of the intrinsic resolution of the detector) if the magnification factor is large enough. Short imaging distances can often be used in pinhole imaging to increase the geometric efficiency of the collimator, but this results in a smaller field-of-view (FOV). Thus, a pinhole collimator coupled to a conventional gamma camera (active detector area normally greater than 300 mm × 300 mm) creates an effective mouse imaging system. Since the size of our proposed detector (64 mm × 40 mm) is only slightly larger than the average mouse, our proposed system cannot benefit from the magnification of a pinhole collimator for whole mice imaging. However, in certain applications where smaller FOV is sufficient (e.g. imaging the heart or brain of a mouse), a pinhole collimator can be used to achieve submillimeter spatial resolution as shown in Fig. 3. Another characteristic of the pinhole collimator (not included in our calculation) is that gamma rays passing through the pinhole aperture and entering the detector at an oblique angle can cause parallax errors due to the depth of interaction (DOI). It has been simulated that for 140 keV gamma rays and 6 mm thick CsI(Tl) scintillator, the loss of spatial resolution due to DOI can contribute 0.3−0.5 mm FWHM [8, 27]. As the interaction length and detector thickness are similar for 140 keV in CsI(Tl) and 27 keV in Si(Li), we would expect similar degradation in the spatial resolution in our proposed system using pinhole collimator.

On the other hand, the geometric efficiency and FOV of a parallel hole collimator do not depend on the imaging distance. With a small enough hole diameter, short enough imaging distance and sufficiently good intrinsic resolution, parallel-hole collimators can achieve good system spatial resolution with reasonable geometric efficiency as shown in Fig. 4. For whole mouse imaging, we propose to use a high-resolution parallel-hole collimators with a square hole width of 0.4 mm, length of 10 mm, and septa thickness of 0.05 mm, giving a system spatial resolution of 1.6 mm FWHM at an imaging distance of 20 mm, and a geometric efficiency of about 10^{-4}. With a detector efficiency of about 90%, this will give a sensitivity of 6.7 cps/μCi for a dual head camera.

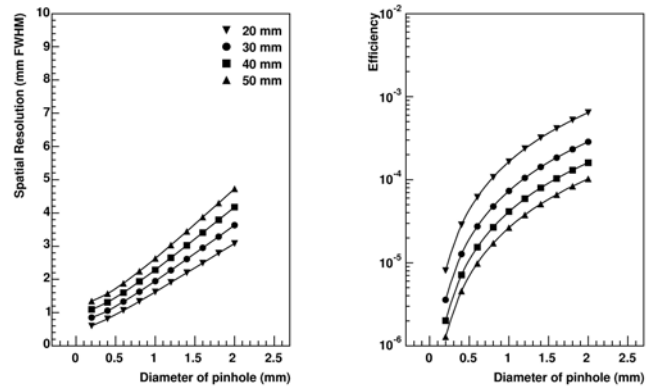

Fig. 3. Spatial resolution and efficiency of tungsten pinhole collimators for 27.5 keV photons as a function of the diameter of the pinhole. The distance from the pinhole aperture to the detector is 40 mm, and the intrinsic resolution of the detector is 1 mm. Curves of different imaging distances are plotted.

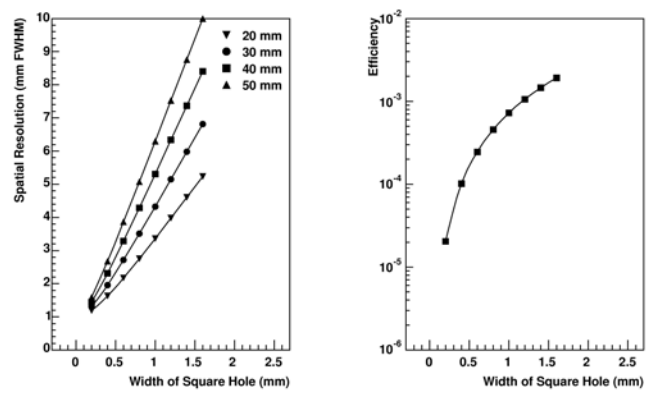

Fig. 4. Spatial resolution and efficiency of tungsten parallel-hole collimators for 27.5 keV photons as a function of the width of the square hole. The geometric length of the collimator is 10 mm, the thickness of the septa is 0.05 mm, the distance from the collimator to the detector is 2 mm, and the intrinsic resolution of the detector is 1 mm. Curves of different imaging distances are plotted. Note that the efficiency of a parallel-hole collimator is independent of the imaging distance.

As a result of the low geometric efficiency of the collimator, the statistical noise is a major limitation of SPECT systems. In order to estimate the minimum number of events needed to obtain a reasonable quality SPECT image, we use the empirical formula derived in [28]. Each of the Si(Li) detectors has 2560 (64 × 40) pixels. Assume that the region of interest occupies 10 pixels and the required contrast is 2-to-1. The root-mean-square (RMS) uncertainty per pixel is set at 20%. With these parameters, the minimum number of events needed is about 1.6 million events. With a 100 μCi injection in a mouse and a system sensitivity of 6.7 cps/μCi, an imaging time of about 60 minutes would be required. The sensitivity of a SPECT system can be improved by using a lower resolution collimator and/or a higher injection dosage, thereby shortening the imaging time and/or improving the statistical noise in the reconstruction.

V. Measurements

To validate our assumptions on the detector performance, measurements were made to estimate the performance for a Si(Li) detector in detecting the emissions of ^{125}I. A single element Si(Li) detector fabricated using the standard LBNL process is used to perform the measurements. The detector is cylindrical in shape. The overall diameter is 24 mm, and the thickness is 6 mm (the same thickness as the proposed detector). The diameter of the active area is 16.5 mm. The n-type contact consists of diffused lithium, while the p-type contact is a gold surface barrier. The detector is operated at a reverse bias voltage of 700 V. The detector is evaluated in a liquid nitrogen cooled cryostat where the detector was cooled to reduce its leakage current. In the measurements presented here, the detector is cooled to about 230 K so that a single channel exhibits a leakage current of about 3 nA to simulate the expected bulk leakage current for a 1 mm x 1 mm x 6 mm (the proposed pixel size) detector element at room temperature. Using a picoammeter, the leakage current of the detector was measured to be 2.8 nA. The detector signal is read out by a custom low-noise charge-sensitive preamplifier built from discrete components [29] followed by a Tennelec TC 244 shaper amplifier. The preamplifier has a peaking time of about 2 μs.

Fig. 5 shows the pulse height spectrum for the Si(Li) detector excited with the emissions of ^{125}I. The total capacitance shunting the input of the preamplifier is measured to be about 17 pF due largely to the total capacitance from the various interconnections (e.g., the connector on the cryostat, the long lead from the detector to the connector, etc) in the experimental setup, which is not ideal. The electronic noise is determined mainly by the leakage current and the input capacitive load on the preamplifier. As the leakage current is similar to what is expected but the input capacitive load is larger, the measurement of the energy resolution represents a pessimistic estimate. The three distinct narrow peaks are the 27.5 keV, 31.0 keV and 35.5 keV emissions of ^{125}I. The broad peak at lower energies is due to photons that have Compton scattered in the material around the detector (e.g., the cryostat cold finger), and are subsequently absorbed in the detector. Fig. 6 and Fig. 7 show the signal amplitude and energy resolution as a function of peaking time respectively. At short peaking times (less than 2 μs) there are significant ballistic deficits causing the signal amplitude to be less than that at long peaking times. Therefore, the energy resolution at short peaking times is significantly poorer. The ballistic deficit is eliminated when the peaking time is above 2−3 μs, achieving the best energy resolution (for 27.5 keV) of 8.5% FWHM for leakage currents of 2.8 nA. The energy resolution increases with increasing peaking time because the parallel noise from the leakage current dominates.

We propose to re-design a custom readout ASIC [22] which is presently optimized for an input load of 5 pF to realize the high electronic channel density required. In practice, the noise performance of a custom ASIC is not necessarily as good as that of a discrete preamplifier. Based on a previous design of another ASIC optimized for high input load [30, 31], we estimate that at a peaking time of 2 μs, a leakage current of 3 nA, and an input capacitive load of 12 pF, the equivalent noise charge is about 460 e^- RMS. Since the Fano factor of Si is small (~0.1) [16], the statistical fluctuation in the number of charge generated by 27.5 keV photons is less than 1% FWHM. Therefore, the expected energy resolution will be about 15% FWHM, which will be dominated by the electronic noise.

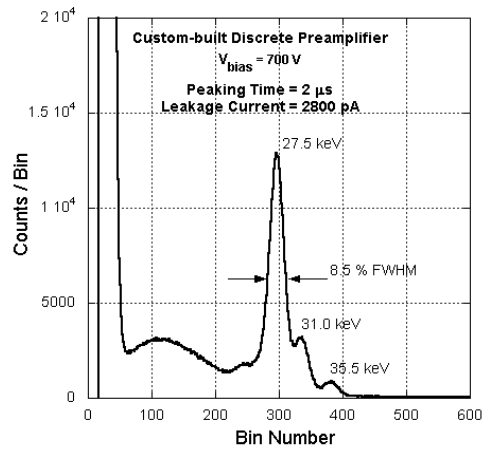

Fig. 5. ^{125}I spectrum read out by the custom-built discrete preamplifier with a peaking time of about 2 μs and a detector leakage current of 2.8 nA. The total capacitance shunting the input of the preamplifier is about 17 pF.

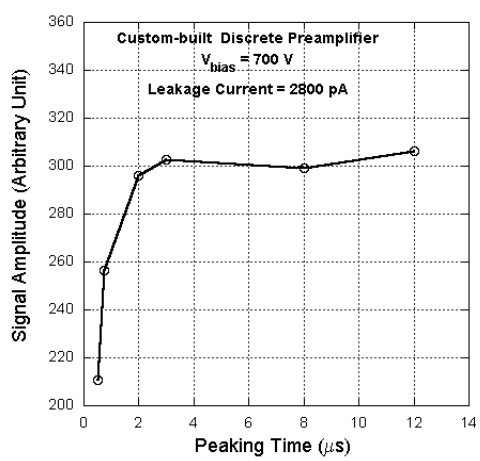

Fig. 6. Signal amplitude of the 27.5 keV emissions of ^{125}I.

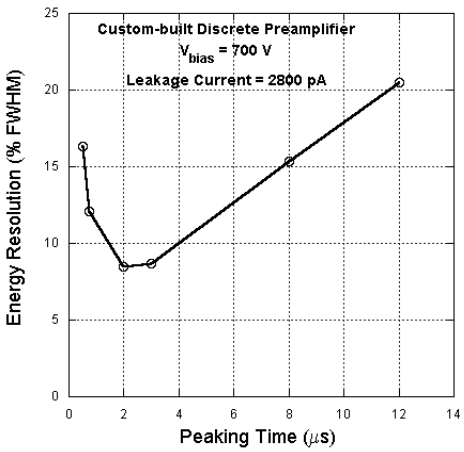

Fig. 7. Energy resolution of the 27.5 keV emissions of ^{125}I.

VI. Conclusions

We have presented a conceptual design for a high-resolution SPECT system using pixellated Si(Li) detectors for *in vivo* ^{125}I imaging. Using a high-resolution parallel-hole collimator, the expected system spatial resolution is 1.6 mm FWHM at an imaging distance of 20 mm, and sensitivity is 6.7 cps/μCi. Our measurements on the detector response to the emissions of ^{125}I show that an energy resolution of 8.5% FWHM can be achieved. Since our proposed readout ASIC will be optimized for our proposed detector system, it is expected to give similar performance. However, based on our conservative estimate of the electronic noise of the proposed readout ASIC, we estimate that our system will have an energy resolution of about 15% FWHM.

VII. References

[1] International Human Genome Sequencing Consortium, "Initial sequencing and analysis of the human genome," *Nature*, vol. 409, pp. 860-921, 2001.

[2] Mouse Genome Sequencing Consortium, "Initial sequencing and comparative analysis of the mouse genome," *Nature*, vol. 420, pp. 520-562, 2002.

[3] T. F. Massoud and S. S. Gambhir, "Molecular imaging in living subjects: seeing fundamental biological processes in a new light," *Genes and Devel*., vol. 17, pp. 545-580, 2003.

[4] S. Y. F. Chu, L. P. Ekstrom, and R. B. Firestone, "WWW Table of Radioactive Isotopes."

[5] NEN Research Products Catalog: PerkinElmer Life and Analytical Sciences, 2003.

[6] Amersham Biosciences Catalog, 2003.

[7] F. A. Dilmanian, D. A. Weber, J. A. Coderre, D. D. Joel, K. G. Shi, G. E. Meinken, *et al*., "A high resolution SPECT system based on a multichannel-plate imager," *IEEE Trans. Nucl. Sci*., vol. 37, pp. 687-695, 1990.

[8] K. Iwata, A. B. Hwang, M. C. Wu, H. R. Tang, A. J. Da Silva, K. H. Wong, *et al*., "Design and utility of a small animal CT/SPECT system," *2001 IEEE Nucl. Sci. Symp. Conf. Rec*., vol. 3, 2002.

[9] F. J. Beekman, D. P. McElroy, F. Berger, S. S. Gambhir, E. J. Hoffman, and S. R. Cherry, "Towards in vivo nuclear microscopy: iodine-125 imaging in mice using micro-pinholes," *Eur. J. Nucl. Med*., vol. 29, pp. 933-938, 2002.

[10] G. A. Kastis, M. C. Wu, S. J. Balzer, D. W. Wilson, L. R. Furenlid, G. Stevenson, et al., "Tomographic small-animal imaging using a high-resolution semiconductor camera," *IEEE Trans. Nucl. Sci*., vol. 49, pp. 172, 2002.

[11] A. G. Weisenberger, R. Wojcik, E. L. Bradley, P. Brewer, S. Majewski, J. Qian, *et al*., "SPECT-CT System for Small Animal Imaging," *IEEE Trans. Nucl. Sci*., vol. 50, pp. 74, 2003.

[12] M. S. Saha, E. L. Bradley, P. Brewer, K. K. Gleason, B. Kross, S. Majewski, *et al*., "Incorporation of a fluoroscopic x-ray modality in a small animal imaging system," *IEEE Trans. Nucl. Sci*., vol. 50, pp. 333, 2003.

[13] T. E. Peterson, D. W. Wilson, and H. H. Barrett, "Application of silicon strip detectors to small-animal imaging," *Nucl. Instr. Meth*., vol. 505, pp. 608-611, 2003.

[14] I. D. Hau, C. Tindall, and P. N. Luke, "New contact development for Si(Li) orthogonal-strip detector," *Nucl. Instr. Meth*., vol. A 505, pp. 148-154, 2003.

[15] A. R. Goode, D. K. Glover, D. D. Watson, G. A. Beller, L. M. Riou, R. Lima, *et al.*, "Application of a small field of view gamma camera based on a 5" PSPMT and crystal scintillator array for high resolution small animal cardiac imaging," *2002 IEEE Nucl. Sci. Symp. Conf. Rec.*, vol. 3, 2003.

[16] G. F. Knoll, *Radiation Detection and Measurement*, 3rd ed. NewYork/Chichester/Weinheim/Brisbane/Singapore/Toronto: John Wiley & Sons, 2000.

[17] S. M. Sze, *Physics of Semiconductor Devices*, 2nd ed. NewYork/Chichester/Weinheim/Brisbane/Toronto/Singapore: John Wiley & Sons, 1981.

[18] Y. Eisen, A. Shor, and I. Mardor, "CdTe and CdZnTe gamma ray detectors for medical and industrial imaging system," *Nucl. Instr. Meth*., vol. A 428, pp. 158, 1999.

[19] D. A. Landis, Y. K. Wong, J. T. Walton, and F. S. Goulding, "Computer controlled drifting of Si(Li) detectors," *IEEE Trans. Nucl. Sci*., vol. 36, pp. 185-189, 1989.

[20] A. Fong, J. T. Walton, E. E. Haller, H. A. Sommer, and J. Guldberg, "Characterization of large diameter silicon low-bias charge collection analysis in Si(Li) PIN diodes," *Nucl. Instr. Meth*., vol. 199, pp. 623-630, 1982.

[21] A. S. Grove, "Physics and Technology of Semiconductor Devices," Wiley, New York, 1974, pp. 174.

[22] M. Pedrali-Noy, G. J. Gruber, B. Krieger, E. Mandelli, G. Meddeler, V. Rosso, et al., "PETRIC - a positron emission tomography readout IC," IEEE Trans. Nucl. Sci., vol. NS-48, pp. 479-484, 2001.

[23] H. Anger, "Radioisotope cameras," in *Instrumention in Nuclear Medicine*, vol. 1, G. J. Hine, Ed. New York: Academic, 1967, pp. 516-517.

[24] H. H. Barrett and W. Swindell, in *Radiological Imaging: TheTheory of Image Formation, Detection and Processing*. NewYork: Academic, 1981, pp. 124-178.

[25] H. O. Anger, "Survey of radioisotope cameras," *ISA Transactions*, vol. 5, pp. 311-334 1966.

[26] E. L. Keller, "Optimum dimensions of parallel-hole, mulit-aperture collimators for gamma-ray cameras," *J. Nucl. Med*., vol. 9, pp. 233-235, 1968.

[27] A. B. Hwang, K. Iwata, and B. H. Hasegawa, "Simulation of depth of interaction effects for pinhole SPECT," *2001 IEEE Nucl. Sci. Symp. Conf. Rec.*, vol. 3, pp. 1293-1297, 2002.

[28] T. F. Budinger, S. E. Derenzo, W. L. Greenberg, G. T. Gullberg, and R. H. Huesman, "Quantitative potentials of dynamic emission computed tomography," *J. Nucl. Med*., vol. 19, pp. 309-315, 1978.

[29] L. Fabris, "Private communication."

[30] V.Re, J. Dewitt, S. Dow, A. Frey, R. P. Johnson, W. Kroeger, *et al.*, "The rad-hard readout system of the BaBar silicon vertex tracker," *Nucl. Instr. Meth*., vol. A409, pp. 354-359, 1998.

[31] E. Mandelli, "Private communication."